

Scale Determines Whether Language Models Organize Representation Geometry for Prediction

Weilun Xu

School of Computer and Communication Sciences

École Polytechnique Fédérale de Lausanne

weilun.xu@epfl.ch

Abstract

In language models, what a representation encodes is determined by the geometry of its representation space: distances, not activations, carry meaning. Existing tools characterize the *shape* of this geometry but do not ask what that shape is organized *for*. We introduce **Subspace PGA**, a metric that tests whether a layer’s distance structure aligns with the readout subspace of the unembedding matrix W_U more than with random subspaces of equal size. Across seven Pythia models (70M–6.9B) and three cross-family models, intermediate geometry is significantly organized for prediction (peak $z = 9$ –24), but the degree is scale-dependent: small models ($d \leq 1024$) progressively lose it at late layers during training—even as loss keeps improving—while large models ($d \geq 2048$) preserve it throughout. We trace this to a capacity trade-off: a few dominant directions migrate away from W_U ’s readout, *masking* rather than destroying the predictive structure beneath, and removing them restores alignment. Neither spectral metrics nor loss curves capture this distinction. Scale thus determines not only how well a model predicts, but how its representation geometry is organized to do so.

1 Introduction

In a language model, what a representation encodes is determined by where it sits relative to other representations (Shepard, 1987; Gärdenfors, 2000): semantic properties appear as linear directions (Marks & Tegmark, 2024; Gurnee & Tegmark, 2024; Li et al., 2023a), concepts form systematic geometric structures (Park et al., 2025), and those structures converge across architectures (Huh et al., 2024). Existing tools describe the *shape* of this geometry—its rank, its spectral decay, its cross-model convergence. None of them ask what that shape is organized *for*.

What is this geometry organized for?

For a language model, the candidate function is prediction. The unembedding matrix W_U maps the final hidden state to a distribution over the next token, and existing theory argues that representations should organize around this output (Crutchfield & Young, 1989; Zhao et al., 2024; Tishby et al., 1999). But theory only constrains the output itself; whether *intermediate* layers also organize their distance structure around prediction is an empirical question. Current tools do not answer it. Spectral metrics characterize shape, not functional orientation (Li et al., 2025). The logit lens (nostalgebraist, 2020) asks whether W_U can decode a single hidden state into the right token—a question about individual points, not about how the *distances between* points are arranged (§2).

We introduce **Subspace PGA** (§3). An SVD of W_U ranks input directions by how strongly W_U responds to them, and the top- k of these directions—which we call the *readout subspace*—are the directions the model uses to produce its predictions. If a layer’s distance structure is organized for prediction, projecting hidden states onto the readout subspace should preserve more of the full-space distance structure than projecting onto an arbitrary k -dimensional subspace. Subspace PGA measures this preservation against a null of 100

arXiv:2605.17084v1 [cs.LG] 16 May 2026

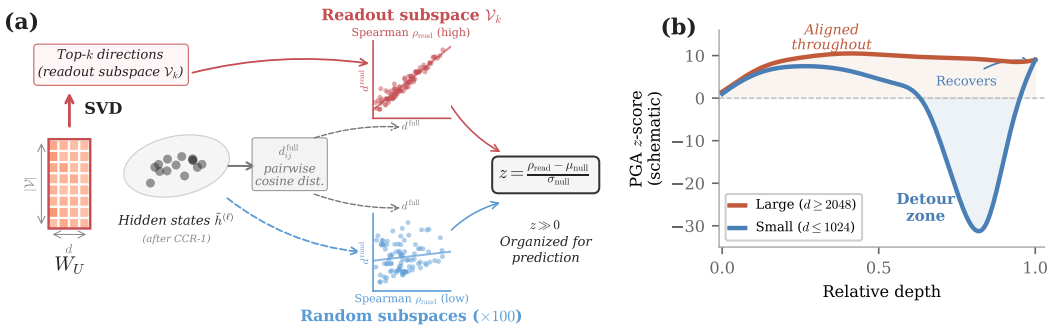


Figure 1: Subspace PGA: Scale Determines Predictive Organization. (a) Method: SVD of the unembedding matrix W_U defines a readout subspace (top- k right singular vectors). We project hidden states onto this subspace and onto 100 random subspaces of equal dimensionality to form a null distribution, then compare how well each projection preserves the full-space distance structure. The z -score quantifies how much more geometric structure lives in prediction-relevant directions than expected by chance. (b) Result: Large models ($d \geq 2048$) maintain predictive organization throughout depth; small models ($d \leq 1024$) lose it at late layers (shaded), then recover at the final layer. Both achieve comparable loss—the distinction is not reliably captured by spectral metrics.

random k -dimensional subspaces, sampled uniformly on the Grassmannian, and reports a z -score: how much more geometric structure concentrates in prediction-relevant directions than chance allows.

Across seven Pythia models (70M–6.9B) (Biderman et al., 2023) and three cross-family models, intermediate geometry is significantly organized for prediction. Peak z -scores reach 9–24 at mid layers, and the organization is established within the first 1,000 training steps (§4.3). It is not, however, maintained uniformly. Small models ($d \leq 1024$) progressively lose it at late layers during training— z falls to -32 in Pythia-410M, even as loss continues to drop—while larger models ($d \geq 2048$) preserve it across all intermediate layers (Figure 1). The mechanism is a capacity trade-off. In a small model’s late layers, the direction of largest variance in the residual stream rotates *away* from the readout subspace; random subspaces then capture as much of the distance structure as the readout one does, and the readout’s privileged status disappears. The predictive structure underneath is *masked*, not destroyed: removing that single dominant direction restores positive z at every layer for all models with $d \geq 768$ (§4.1). Two regimes emerge. Large models keep their geometry aligned with prediction at every depth (*direct*). Small models detour through prediction-irrelevant directions before the final layer projects them back (*detour*). Both achieve comparable loss, and no spectral metric we tested separates them (§4.2).

Contributions. (1) Subspace PGA: a metric that quantifies how much of a layer’s distance structure concentrates in W_U ’s readout directions, against a dimensionality-matched random null (§3). (2) Predictive organization is scale-dependent. Small models develop a detour at late layers; large models do not. Loss curves and spectral metrics miss this distinction (§4, §4.2). (3) The detour is a capacity trade-off, not a learned routing. The dominant variance direction migrates away from the readout during training, and removing it restores alignment (§4.1, §4.3). (4) The readout subspace concentrates cross-architecture convergent structure, anchoring representational convergence to predictive function (§4.4).

2 Related Work

Predictive Geometry Computational mechanics (Crutchfield & Young, 1989) and ϵ -machines predict grouping by conditional futures. Shai et al. (2024) confirmed this in HMM-trained transformers; Zhao et al. (2024) proved a formal analogue for NTP. The information bottleneck (Tishby et al., 1999; Shwartz-Ziv & Tishby, 2017) and compression–prediction

equivalence (Delétang et al., 2024) suggest compression toward predictive-relevant directions. Saurez et al. (2026) prove that any feature decoded through a linear interface must occupy an invariant linear subspace of that interface, grounding why readout alignment should exist. These works imply predictive organization but provide no per-layer metric for its degree.

Spectral Geometry Li et al. (2025) tracked RankMe and α -ReQ across training, identifying geometric phases (warmup, entropy-seeking, compression-seeking). The Platonic Representation Hypothesis (Huh et al., 2024) argues that representations converge across models and modalities; Lee et al. (2025) showed that embedding geometry has shared global and local structure. These works describe the shape of representation geometry; Subspace PGA asks whether that shape is oriented toward the model’s predictive task.

Intermediate Layer Analysis The logit lens (nostalgebraist, 2020) and tuned lens (Belrose et al., 2023) decode intermediate predictions; the tuned lens requires learned affine corrections, demonstrating “representational drift.” Skean et al. (2025) showed that intermediate layers outperform the final layer on downstream tasks by up to 16% (ICML 2025). The logit lens measures absolute decodability (does W_U produce the right token?); Subspace PGA measures geometric organization (is the distance structure aligned with W_U ?). Logit lens failure occurs at intermediate layers in *all* models, while loss of predictive organization is specific to small models—these are distinct phenomena (Appendix D.3).

Representation Collapse and Degeneration Dong et al. (2021) showed self-attention loses rank doubly exponentially with depth; Gao et al. (2019) identified representation degeneration; Arefin et al. (2025) showed that preventing intermediate-layer collapse improves reasoning. The loss of predictive organization we observe is distinct (§4.1): representations retain substantial diversity ($\rho > 0.50$), and the phenomenon is a consequence of scale, not a pathology requiring regularization.

Unembedding Subspace Analysis Cancedda (2024) used SVD of the unembedding matrix to partition logit outputs into spectral bands, revealing a “dark subspace” of tail singular vectors that drives attention sink behavior. Dar et al. (2023) treat the embedding space as a universal reference frame for interpreting transformer computations. Subspace PGA builds on this intuition but asks a different question: whether the *distance structure* of hidden states is organized along readout directions, not whether specific computations occur in particular subspaces. The dimensionality-matched random-subspace null is what reveals the scale-dependent loss of organization. Kulkarni et al. (2026) study the effective rank of W_U across 108 models, finding spectral properties alone insufficient to predict performance—consistent with our finding that spectral metrics do not capture predictive organization.

3 Methods

3.1 Subspace Predictive-Geometric Alignment

Readout subspace. Let $W_U = U\Sigma V^\top$ be the SVD of the unembedding matrix. The right singular vectors V live in hidden space, and the singular values σ_i measure how strongly W_U amplifies each direction. We define the *readout subspace* \mathcal{V}_k as the span of the top- k right singular vectors—the k directions W_U amplifies most. A vector orthogonal to \mathcal{V}_k contributes nothing to the top- k logits the readout produces, and so does no work toward the model’s predictions.

Distance preservation. For a layer ℓ and n contexts, we take the anisotropy-corrected last-token hidden states $\{\tilde{h}_i\}$ (§3.2) and compute pairwise cosine distances in the full hidden space and in the readout subspace:

$$d_{ij}^{\text{full}} = 1 - \frac{\tilde{h}_i \cdot \tilde{h}_j}{\|\tilde{h}_i\| \|\tilde{h}_j\|}, \quad d_{ij}^{\text{proj}} = 1 - \frac{(P_k \tilde{h}_i) \cdot (P_k \tilde{h}_j)}{\|P_k \tilde{h}_i\| \|P_k \tilde{h}_j\|}, \tag{1}$$

where P_k projects onto \mathcal{V}_k . The full distance is how far apart hidden states are in the original geometry; the projected distance is how far apart they are when only readout-relevant directions are visible. The *readout correlation* is the Spearman rank correlation between the two,

$$\rho_{\text{readout}}^{(\ell)} = \rho_{\text{Spearman}}(\mathbf{d}^{\text{full}}, \mathbf{d}^{\text{proj}}), \tag{2}$$

and tells us how much of the layer’s distance structure survives after we throw away everything outside \mathcal{V}_k .

Random null and the z-score. ρ_{readout} alone is hard to interpret: any sufficiently high-dimensional projection preserves *some* structure. To isolate the readout’s contribution we compare against a null formed by drawing 100 uniformly random orthonormal k -dimensional subspaces (via QR of a $d \times k$ Gaussian matrix), each yielding a correlation ρ_b . Subspace PGA is the resulting z-score:

$$\text{PGA}^{(\ell)} = z^{(\ell)} = \frac{\rho_{\text{readout}}^{(\ell)} - \mu_{\text{null}}^{(\ell)}}{\sigma_{\text{null}}^{(\ell)}}. \tag{3}$$

z measures how privileged the readout directions are over arbitrary k -dimensional subspaces. $z \gg 0$: the readout captures more of the layer’s distance structure than a random k -dimensional subspace would—the geometry concentrates in prediction-relevant directions. $z \approx 0$: the readout is no better than chance. $z < 0$: random subspaces preserve more structure than the readout does, and the readout has lost its privileged status. The construction parallels representational similarity analysis (Kriegeskorte et al., 2008) in form, with one of the two compared spaces replaced by a functionally defined subspace and the other by a dimensionality-matched random null. A JSD-based variant for comparing content types (rather than learned vs. random readouts) is in Appendix D.1.

3.2 Anisotropy Correction

Transformer hidden states are anisotropic (Ethayarajh, 2019): a single direction in the residual stream typically dominates the variance and inflates cosine similarity between unrelated states. This biases z asymmetrically. The dominant direction enters the readout and the random subspaces unequally—both inherit it, but the readout inherits it differently—so z measured on raw hidden states confounds geometric organization with global anisotropy.

We remove this confound with mean-centering plus CCR-1 (Mu et al., 2018):

$$\tilde{h} = h - \mu, \quad \tilde{h} = \tilde{h} - (\tilde{h} \cdot v_1) v_1,$$

where μ is the mean hidden state and v_1 is the leading right singular vector of the centered representation matrix. After correction, pairwise isotropy reaches ≥ 0.99 at every layer of every model (Appendix C.2).

CCR-1 itself could in principle remove readout-aligned variance and bias z in the opposite direction. Empirically it does not: at the layers where z goes negative in small models, the CCR-1 direction lies largely outside the readout subspace ($\|P_k v_1\| \approx 0.13$ for Pythia-410M L6–L23, ≈ 0.25 for Pythia-1B), and is more aligned with the readout at the final layer (≈ 0.42 – 0.55 , where $z > 0$). CCR-1 therefore removes a direction that lies mostly outside the readout at the layers where collapse occurs, so any change in z after correction reflects geometric reorganization rather than removal of readout-aligned variance. Full per-layer values are in Appendix C.3.

3.3 Experimental Setup

Models. Our primary suite is the seven Pythia models from 70M to 6.9B (Biderman et al., 2023), all trained on the same data (The Pile) with the same tokenizer (GPT-NeoX), so capacity is the only variable across the suite (full d/L in Table 2). Pythia uses *untied* embeddings, which matters here: tied embeddings make layer-0 hidden states identical to the input embeddings and therefore trivially aligned with W_U , inflating early-layer z -scores.

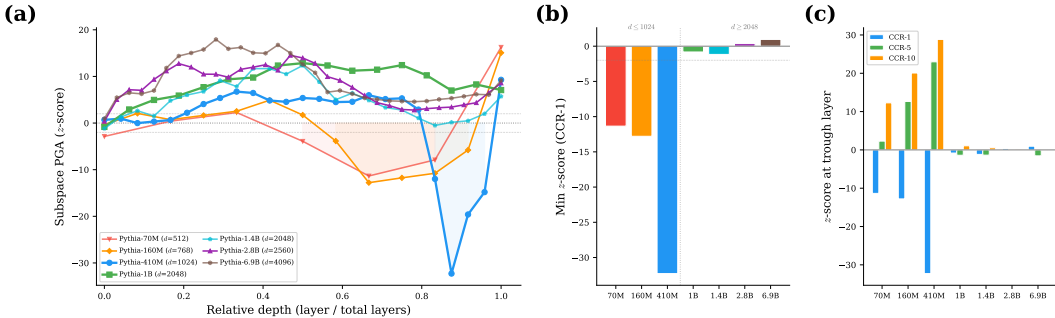


Figure 2: **Scale Determines Predictive Organization.** (a) Subspace PGA z-score vs. relative depth. Small models (warm) lose predictive organization at late layers before recovering at the final layer; large models (cool) maintain it throughout. (b) Minimum z-score across the suite: a sharp transition at $d \approx 2048$. (c) Under CCR-5/10, all negative z-scores become positive for $d \geq 768$ —predictive structure is intact but masked.

The 1B / 1.4B pair shares width but differs in depth, isolating depth’s contribution. For cross-family validation we use OLMo-1B (Groeneveld et al., 2024), Phi-1.5 (Li et al., 2023b), and Gemma-2-2B (Gemma Team, 2024), spanning both tied and untied readouts.

Data. We sample 1,000 contexts from OpenWebText with ≥ 64 tokens, truncated to 512. The same texts are used for every model, so hidden-state samples differ only in the model that produced them.

Computation. For each model and layer, we extract the last-token hidden state of each context, apply mean + CCR-1 correction, and compute Subspace PGA with $k = 100$ readout dimensions and 100 random subspaces. We also compute spectral metrics (RankMe, stable rank, participation ratio, α -ReQ, isotropy, condition number, TwoNN intrinsic dimensionality) for the comparison in §4.2. Final-layer states are taken post-LayerNorm, matching the geometry W_U operates on.

Readout coverage. Fixing $k=100$ means the readout subspace covers a much larger fraction of W_U ’s variance in small models than in large ones (Appendix C.4). Higher coverage favors a positive z , so the observed loss of predictive organization in the smallest models happens despite the most favorable conditions for alignment—a conservative finding rather than an artifact of fixing $k = 100$.

4 Results

4.1 Prediction Shapes Geometry—but Not Uniformly

Across all models with at least 12 layers, mid-layer geometry is significantly organized for prediction: readout-subspace distances preserve far more of the full-space distance structure than random subspaces do, with peak z-scores between 9 and 24 (Figure 2a; per-layer values in Appendix B.2). This is consistent with theory that next-token prediction shapes representations around the readout (Crutchfield & Young, 1989; Zhao et al., 2024). But the organization is not maintained uniformly with depth, and how it breaks down depends on scale.

Late-layer collapse. In Pythia-160M and 410M, predictive organization collapses at late-but-not-final layers (Figure 2a, shaded). What is striking is the regularity. Both models recover at the very last layer, and both collapse zones occupy roughly the same relative depth (≈ 65 – 95% of total layers). Collapse followed by recovery means the final layer is undoing what intermediate layers did—redirecting geometry back toward W_U after a stretch of computation that pulled it away. We call this trajectory a *detour*.

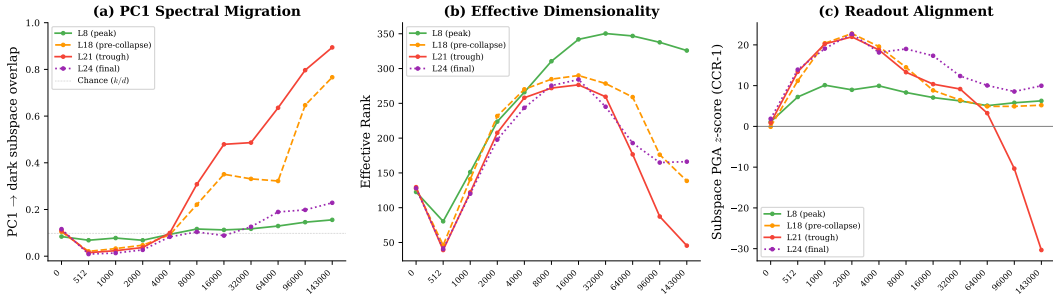


Figure 3: **PC1 Migrates Bright → Dark as Collapse Emerges (Pythia-410M).** (a) PC1’s dark-subspace overlap increases at late layers during training; the final layer stays anchored. (b) Effective rank drops as anisotropy concentrates on dark directions. (c) z -score goes negative when $\text{PC1} \rightarrow \text{dark} > 0.80$ and effective rank < 100 .

Mechanism. What does collapse look like at the level of correlations? In the affected layers, the readout correlation ρ_{readout} stays moderate ($\approx 0.50\text{--}0.74$), so distance information has not vanished from \mathcal{V}_k . The random-subspace correlation μ_{null} , however, rises to $\approx 0.80\text{--}0.90$: an arbitrary k -dimensional subspace now captures the layer’s distance structure as well as the readout does. The readout’s privileged status disappears. The predictive structure is not destroyed—it is *overwhelmed*.

To see why, consider the dominant variance direction. Following Cancedda (2024), we partition hidden space into the readout subspace \mathcal{V}_k (the “bright” directions, where W_U acts) and its orthogonal complement (the “dark” directions, which W_U ignores). Across training, PC1 of the residual stream gradually rotates from bright into dark at late layers (Figure 3a, b). When PC1 is bright, both the readout and a typical random subspace pick up its variance, and ρ_{readout} stays above μ_{null} . When PC1 is dark, random subspaces still pick up a fraction k/d of its variance but the readout picks up almost none, so μ_{null} rises while ρ_{readout} does not, and z goes negative (Figure 3c).

This accounts for how collapse looks but not why it happens only in small models. Pythia-1B undergoes comparable PC1 migration yet z stays positive (§4.3). The simplest explanation is capacity: small models lack enough dimensions to host a dominant variance direction for intermediate computation *and* a separate set of readout-aligned directions, so the two collide; large models have room for both. Removing the top one or few principal components (CCR-5, CCR-10) restores positive z at every layer of every model with $d \geq 768$ (Figure 2c)—the predictive structure was never erased; it was sitting under a thin layer of dominant-direction variance that masked it.

Robustness. Results are stable across $k \in \{50, 100, 200\}$ and $k = d/10$, bootstrap resampling, and random seeds (Appendices C.3–C.6). *Orthogonal* PGA—the same metric computed in \mathcal{V}_k^\perp —never exceeds the random null at any model-layer combination tested (0/12; Appendix A), so the alignment really is concentrated in \mathcal{V}_k rather than diffused across hidden space. Replacing W_U with the input embedding W_E yields z -scores indistinguishable from random (Appendix C.8), so the alignment is specific to the predictive interface and not an artifact of any matrix the model contains.

4.2 Spectral Metrics Are Blind to Predictive Organization

Spectral metrics describe the shape of representation geometry; Subspace PGA describes what that shape is organized for. The two are largely independent. Across the Pythia suite, no spectral metric we tested—RankMe, stable rank, participation ratio, α -ReQ, isotropy, condition number, TwoNN intrinsic dimensionality—reliably tracks z . Whatever correlation a metric has with z in one model disappears in another (Appendix D.4, Figure 8). The cleanest illustration is Pythia-410M’s collapse zone (L20–L23), where α -ReQ is indistinguishable

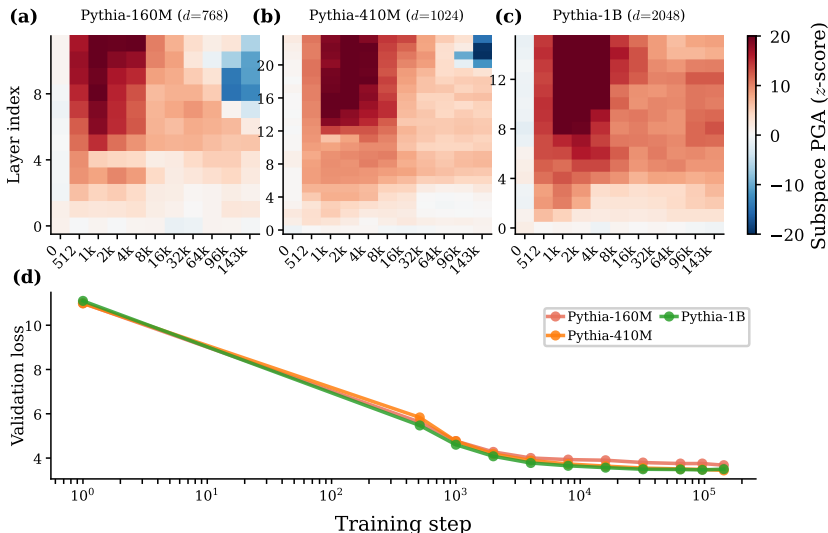


Figure 4: **Masking is learned and scale-dependent.** z-score across training steps and layers for (a) 160M, (b) 410M, (c) 1B. Small models develop late-layer masking by step $\sim 96k$; 1B never does. (d) Validation loss converges comparably—masking does not affect the training objective.

from surrounding layers while z swings by more than 40 standard deviations. Two layers can have the same shape and be doing very different things with it.

4.3 Training Dynamics: Organization First, Masking Later

Tracking Subspace PGA across 143,000 training steps shows that the late-layer collapse is not built into the architecture: it emerges during training, and whether it emerges at all depends on scale (Figure 4; Tables 3, 4).

Default organization. All three checkpointed models (160M, 410M, 1B) organize geometry along predictive directions within the first 1,000 steps, with most layers reaching $z > 2$ regardless of scale. The direct regime is what training establishes first.

Progressive masking. In the small models ($d \leq 1024$), the dominant variance direction at late layers begins to drift away from the readout around step $\sim 96k$ (Figure 4a, b), and z at those layers drops below zero. The timing coincides with the “compression-seeking” phase of Li et al. (2025), in which effective rank declines and a few directions dominate the residual stream—if those directions point away from \mathcal{V}_k , masking follows. The final layer is held in place by the cross-entropy loss and does not participate in the drift. Pythia-1B undergoes comparable PC migration but never crosses into negative z (Figure 4c), consistent with the capacity reading.

Loss is blind. Validation loss descends smoothly and similarly across all three models (Figure 4d). The collapse leaves no fingerprint on loss, because the training objective constrains only the final readout, not how intermediate layers organize themselves.

4.4 Convergent Structure Concentrates in Predictive Directions

If representation geometry encodes structure that converges across architectures (Huh et al., 2024; Lee et al., 2025), and the readout subspace is the part of that geometry tied to a specific function, then convergence should be most pronounced there. We test this with cross-model RSA: for each pair from {Pythia-1B, OLMo-1B, Phi-1.5}, we compare the Spearman correlation of pairwise distances in the full 2,048-dimensional space against the same correlation in the 100-dimensional readout subspace.

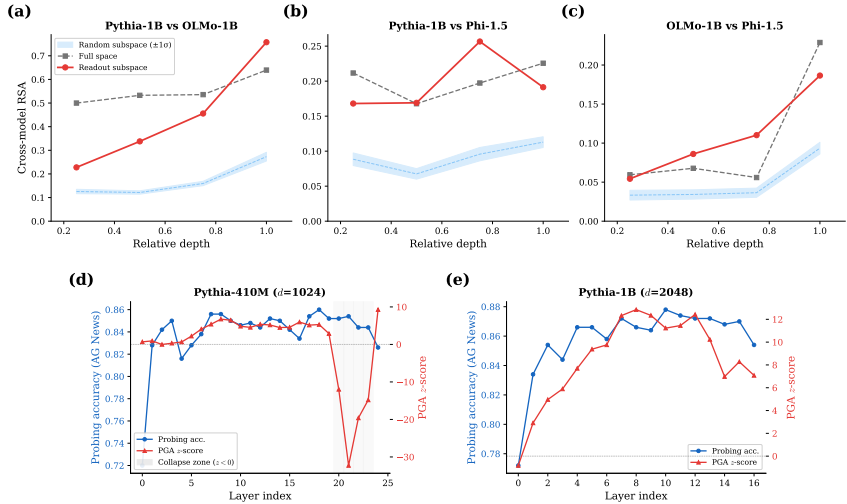


Figure 5: **Convergence and Probing.** (a–c) Cross-model RSA: readout RSA (red) exceeds random null (blue) and sometimes full-space RSA (grey). (d) 410M: probing accuracy stays high in the collapse zone—masking, not erasure. (e) 1B: z-scores and probing accuracy correlate ($\rho = 0.69, p = 0.002$).

The readout subspace does not merely inherit cross-model agreement; it concentrates it (Figure 5a–c). The 100-dimensional readout-RSA exceeds the random-subspace null in all three pairs, and in several pairs exceeds even the full 2,048-dimensional space RSA. The readout appears to filter out model-specific variance that dilutes cross-model agreement in the ambient space. What independently trained models agree on, geometrically, is the part anchored to predictive function. The test is run at one scale with models of similar capacity, so we cannot say whether this generalizes across scale gaps; a stronger causal test (e.g., model stitching; Bansal et al., 2021) would establish whether this convergent structure is sufficient for cross-model substitution.

4.5 Does Predictive Organization Predict Downstream Utility?

To check whether z tracks something that matters beyond geometry, we trained linear probes for AG News topic classification on per-layer hidden states of Pythia-410M and 1B, and compared probe accuracy to Subspace PGA z-scores (Figure 5d–e).

In the geometrically stable Pythia-1B, z and probing accuracy track each other layer by layer ($\rho = 0.69, p = 0.002$): the same layers that organize their distance structure for prediction also yield more linearly separable features for an unrelated downstream task. This makes Subspace PGA usable as a task-free signal for layer selection.

In Pythia-410M, the collapse zone tells the complementary story. Probe accuracy stays around 0.85 even at layers where z falls well below zero. The information needed for the probe is still present in those layers; what changed is its alignment with W_U . This is direct evidence for the masking interpretation in §4.1: the detour reorganizes geometry relative to prediction without erasing the underlying features.

5 Discussion

5.1 What Scale Buys: Two Geometric Regimes

The findings in §4 pick out two regimes, determined by model width.

Direct regime (large models, $d \geq 2048$). Enough representational capacity to host both a large-variance direction for intermediate computation and a separate set of readout-aligned directions. Geometry stays organized for prediction across all intermediate layers.

Detour regime (small models, $d < 1024$). Late layers develop a dominant variance direction that points away from the readout subspace. This is a side effect of limited capacity, not an explicitly learned routing: when a small model has to fit both a large-variance computation and a readout-aligned representation in the same residual stream, the two collide. The final layer projects geometry back into readout-relevant directions, recovering predictive organization at the output.

Both regimes achieve comparable loss, but only the direct one keeps intermediate geometry oriented toward prediction. The distinction is visible to Subspace PGA, but neither loss curves nor any spectral metric we tested reliably surfaces it.

If representation geometry is the medium through which models encode what they “know” (Marks & Tegmark, 2024; Li et al., 2023a), and if this geometry converges across architectures (Huh et al., 2024), then asking what geometry is organized *for* matters as much as characterizing its shape. The cross-model analysis in §4.4 adds to this: convergence concentrates in predictive directions rather than spreading across the ambient hidden space, so what independently trained models agree on geometrically is tied to predictive function (Worrall, 1989).

Three observations point to capacity, not architecture, as the decisive factor. (i) PC1 migrates comparably across scales (§4.3, Figure 4c), so what differs is not whether the migration happens but whether the model has enough remaining dimensions to absorb it. (ii) The Pythia 1B / 1.4B pair shares width but differs in depth: 1.4B shows borderline loss at L20 while 1B does not, so depth gives anisotropy more time to accumulate but does not by itself create the regime. (iii) KL projection of late-layer hidden states onto \mathcal{V}_k shows the collapse zone preserves task-relevant information (Appendix D.5), so the detour reorganizes geometry without changing what is computed.

5.2 Cross-Architecture Validation

Three cross-family models test whether the regime structure depends on Pythia-specific choices.

Untied. Phi-1.5 shows no late-layer loss, consistent with the $d \geq 2048$ threshold generalizing beyond Pythia. Its z-scores are uniformly stronger than Pythia-1.4B’s at matching dimensions, suggesting factors beyond capacity may also matter, though we cannot disentangle them here.

Tied. OLMo-1B shows no loss at any layer. Gemma-2-2B shows no *intermediate*-layer loss, but the final layer collapses via the same PC1-into-dark mechanism. Tying makes W_U share parameters with the input embedding, and this dual constraint may manifest specifically at the output, though we do not test this directly.

5.3 Practical Implications

For practitioners using intermediate hidden states from a language model:

Layer selection in large models. Subspace PGA provides a task-free criterion: in Pythia-1B, layers with the highest z yield the most linearly separable features for AG News topic classification (§4.5). No labelled data are required to compute z , so it can be used to pre-select layers before any probe is trained.

Layer selection in small models. Collapse-zone layers remain usable for probing—probe accuracy is largely unaffected by collapse—but methods that rely on W_U (the logit lens in particular) will fail there because the geometry is misaligned with the readout. Layer selection in small models should account for geometric orientation, not just decodability.

Logit lens vs. predictive organization. These are distinct phenomena even though both involve W_U . Logit-lens failure is universal across scales: every model we tested decodes

intermediate hidden states poorly (Appendix D.3). Loss of predictive organization is specific to small models. A layer can be undecodable while still having geometry aligned with W_U , and vice versa.

5.4 Limitations

Metric scope. Subspace PGA assumes a linear readout. Features routed nonlinearly before W_U (cf. tuned lens; Belrose et al., 2023) may not be captured, and whether a per-layer affine readout would eliminate the collapse remains open. Tied embeddings inflate early-layer alignment trivially. SSMS and MoEs use W_U differently and would need a separate analysis.

CCR sensitivity. Negative z-scores disappear under CCR-5. We read this as informative rather than as an artifact: it shows the collapse is driven by a few dominant masking dimensions, not by an absence of predictive structure. The choice of correction strength determines the object of study.

Generalization. We test up to 6.9B parameters; frontier-scale models are untested. Collapse below $d = 1024$ is observed only in Pythia. Probing uses one task (AG News), and measurements come from final-token hidden states only (Valeriani et al., 2023).

Causality. We observe a geometric pattern, not a causal mechanism. KL projection provides partial evidence that the collapse zone reorganizes rather than recomputes (Appendix D.5); a stronger test—e.g., rotating PC1 back into \mathcal{V}_k and measuring downstream effects—is left to future work. Large $|z|$ values come partly from a low null variance, but absolute ρ values confirm substantive effects (Appendix C.5).

6 Conclusion

We introduced Subspace PGA to ask what representation geometry is organized *for*—a question that spectral metrics, which describe shape alone, do not address.

The answer is prediction, but the degree depends on scale. Small models progressively lose predictive organization at late layers during training, even as loss keeps improving; large models maintain it across all intermediate layers. The lost organization is masked, not erased: removing the dominant variance direction restores it. The same readout subspace also concentrates cross-architecture convergent structure, tying representational convergence to predictive function.

Scale determines not just how well a model predicts, but how its geometry is organized to do so. The difference between functionally coherent and functionally detoured representations is invisible to loss curves and spectral metrics; it surfaces when we ask not what shape geometry takes, but what shape it is organized for.

Reproducibility Statement

All models are publicly available on HuggingFace (Pythia suite from EleutherAI, OLMo-1B from AI2, Phi-1.5 from Microsoft, Gemma-2-2B from Google). Evaluation uses $N=1,000$ OpenWebText contexts (≥ 64 tokens, truncated to 512), readout subspace dimension $k=100$, and 100 random-subspace draws per layer. Anisotropy correction is mean-centering followed by CCR-1. Statistical significance uses Mantel permutation tests ($B=1,000$). Results are stable across random seeds and sample sizes (Appendix C.7). Total compute: ~ 60 – 80 A100 GPU-hours. Code will be released upon acceptance.

References

- Md Rifat Arefin, Gopeshh Subbaraj, Nicolas Gontier, Yann LeCun, Irina Rish, Ravid Shwartz-Ziv, and Christopher Pal. Seq-VCR: Preventing collapse in intermediate transformer representations for enhanced reasoning. In *International Conference on Learning Representations*, 2025. arXiv:2411.02344.
- Yamini Bansal, Preetum Nakkiran, and Boaz Barak. Revisiting model stitching to compare neural representations. In *Advances in Neural Information Processing Systems*, volume 34, 2021.
- Nora Belrose, Zach Furman, Logan Smith, Danny Halawi, Igor Ostrovsky, Lev McKinney, Stella Biderman, and Jacob Steinhardt. Eliciting latent predictions from transformers with the tuned lens. *arXiv preprint arXiv:2303.08112*, 2023.
- Stella Biderman, Hailey Schoelkopf, Quentin Anthony, Herbie Bradley, Kyle O’Brien, Eric Hallahan, Mohammad Aflah Khan, Shivanshu Purohit, et al. Pythia: A suite for analyzing large language models across training and scaling. In *International Conference on Machine Learning*, pp. 2397–2430, 2023.
- Nicola Cancedda. Spectral filters, dark signals, and attention sinks. In *Proceedings of the 62nd Annual Meeting of the Association for Computational Linguistics*, 2024.
- James P Crutchfield and Karl Young. Inferring statistical complexity. *Physical Review Letters*, 63(2):105–108, 1989.
- Guy Dar, Mor Geva, Ankit Gupta, and Jonathan Berant. Analyzing transformers in embedding space. In *Proceedings of the 61st Annual Meeting of the Association for Computational Linguistics*, 2023.
- Grégoire Delétang, Anian Ruoss, Paul-Ambroise Duquenne, Elliot Catt, Tim Genewein, Christopher Mattern, Jordi Grau-Moya, Shane Legg Li, and Joel Veness. Language modeling is compression. In *International Conference on Learning Representations*, 2024.
- Yihe Dong, Jean-Baptiste Cordonnier, and Andreas Loukas. Attention is not all you need: Pure attention loses rank doubly exponentially with depth. In *International Conference on Machine Learning*, pp. 2793–2803, 2021.
- Kawin Ethayarajh. How contextual are contextualized word representations? comparing the geometry of BERT, ELMo, and GPT-2 embeddings. In *Empirical Methods in Natural Language Processing*, pp. 55–65, 2019.
- Jun Gao, Di He, Xu Tan, Tao Qin, Liwei Wang, and Tie-Yan Liu. Representation degeneration problem in training natural language generation models. In *International Conference on Learning Representations*, 2019.
- Peter Gärdenfors. *Conceptual Spaces: The Geometry of Thought*. MIT Press, 2000.
- Gemma Team. Gemma 2: Improving open language models at a practical size. *arXiv preprint arXiv:2408.00118*, 2024.
- Dirk Groeneveld, Iz Beltagy, Pete Walsh, Akshita Bhagia, Rodney Kinney, Oyvind Tafjord, et al. OLMo: Accelerating the science of language models. In *Proceedings of the 62nd Annual Meeting of the Association for Computational Linguistics (Volume 1: Long Papers)*, 2024.
- Wes Gurnee and Max Tegmark. Language models represent space and time. In *International Conference on Learning Representations*, 2024.
- Minyoung Huh, Brian Cheung, Tongzhou Wang, and Phillip Isola. Position: The platonic representation hypothesis. In *International Conference on Machine Learning*, volume 235, pp. 20617–20642, 2024.
- Nikolaus Kriegeskorte, Marieke Mur, and Peter A Bandettini. Representational similarity analysis—connecting the branches of systems neuroscience. *Frontiers in Systems Neuroscience*, 2:4, 2008.

- Atharva Kulkarni, Jacob Mitchell Springer, Arjun Subramonian, and Swabha Swayamdiha. Disentangling geometry, performance, and training in language models. *arXiv preprint arXiv:2602.20433*, 2026.
- Andrew Lee, Melanie Weber, Fernanda Viégas, and Martin Wattenberg. Shared global and local geometry of language model embeddings. In *Conference on Language Modeling*, 2025. Outstanding Paper Award.
- Kenneth Li, Aspen K Hopkins, David Bau, Fernanda Viégas, Hanspeter Pfister, and Martin Wattenberg. Emergent world representations: Exploring a sequence model trained on a synthetic task. In *International Conference on Learning Representations*, 2023a.
- Melody Zixuan Li et al. Tracing the representation geometry of language models from pretraining to post-training. In *Advances in Neural Information Processing Systems*, 2025. arXiv:2509.23024.
- Yuanzhi Li, Sébastien Bubeck, Ronen Eldan, Allie Del Giorno, Suriya Gunasekar, and Yin Tat Lee. Textbooks are all you need II: phi-1.5 technical report. *arXiv preprint arXiv:2309.05463*, 2023b.
- Nathan Mantel. The detection of disease clustering and a generalized regression approach. *Cancer Research*, 27(2):209–220, 1967.
- Samuel Marks and Max Tegmark. The geometry of truth: Emergent linear structure in large language model representations of true/false datasets. In *Conference on Language Modeling*, 2024.
- Jiaqi Mu, Suma Bhat, and Pramod Viswanath. All-but-the-top: Simple and effective postprocessing for word representations. In *International Conference on Learning Representations*, 2018.
- nostalgebraist. interpreting GPT: the logit lens. LessWrong, 2020. URL <https://www.lesswrong.com/posts/AcKRB8wDpdaN6v6ru/interpreting-gpt-the-logit-lens>. Accessed: 2026-03-30.
- Kiho Park, Yo Joong Choe, and Victor Veitch. The linear representation hypothesis and the geometry of large language models. In *International Conference on Machine Learning*, volume 235, pp. 39643–39666, 2024.
- Kiho Park, Yo Joong Choe, and Victor Veitch. The geometry of categorical and hierarchical concepts in large language models. In *ICLR*, 2025. Oral; arXiv:2406.01506.
- Andres Saurez, Yousung Lee, and Dongsoo Har. Why linear interpretability works: Invariant subspaces as a result of architectural constraints. *arXiv preprint arXiv:2602.09783*, 2026.
- Adam Shai, Lucas Teixeira, Alexander Gietelink Oldenziel, Sarah E Marzen, and Paul M Riechers. Transformers represent belief state geometry in their residual stream. In *Advances in Neural Information Processing Systems*, 2024.
- Roger N Shepard. Toward a universal law of generalization for psychological science. *Science*, 237(4820):1317–1323, 1987.
- Ravid Shwartz-Ziv and Naftali Tishby. Opening the black box of deep neural networks via information. *arXiv preprint arXiv:1703.00810*, 2017.
- Oscar Skean, Md Rifat Arefin, Dan Zhao, Niket Patel, Jalal Naghiyev, Yann LeCun, and Ravid Shwartz-Ziv. Layer by layer: Uncovering hidden representations in language models. In *International Conference on Machine Learning*, 2025. Oral; arXiv:2502.02013.
- Naftali Tishby, Fernando C Pereira, and William Bialek. The information bottleneck method. In *Proceedings of the 37th Annual Allerton Conference on Communication, Control, and Computing*, pp. 368–377, 1999.

Lorenzo Valeriani, Diego Doimo, Francesca Cuturello, Alessandro Laio, Alessio Ansuini, and Alberto Cazzaniga. The geometry of hidden representations of large transformer models. In *Advances in Neural Information Processing Systems*, volume 36, 2023.

John Worrall. Structural realism: The best of both worlds? *Dialectica*, 43(1-2):99–124, 1989.

Yize Zhao, Tina Behnia, Vala Vakilian, and Christos Thrampoulidis. Implicit geometry of next-token prediction: From language sparsity patterns to model representations. In *Conference on Language Modeling*, 2024. arXiv:2408.15417.

A Predictive Structure Concentrates in Readout Directions

Predictive organization concentrates in readout-aligned directions. Orthogonal PGA—computed in the complement of the readout subspace—never exceeds the 95th percentile of dimensionality-matched random subspaces at any model \times layer combination (0/12; Table 1). In Pythia-410M, the orthogonal subspace retains 75–80% of representation variance yet carries no above-chance predictive alignment. The readout subspace has lower intrinsic dimensionality ($ID_{\text{readout}} = 18.5$ vs. $ID_{\text{ortho}} = 27.4$ at the final layer), consistent with compression into a predictive manifold.

Models commit to final predictions only in the last layers: intermediate-to-final prediction correlation $\rho < 0.5$ through $\approx 80\%$ depth, then rises sharply to $\rho \approx 1.0$. The timing of this commitment overlaps with the collapse zone in small models.

Table 1: **Orthogonal PGA.** Computed within the complement of the readout subspace, predictive organization never exceeds the 95th percentile of random draws (0/12). The geometry in the complementary space carries no above-chance alignment with the readout.

MODEL	DEPTH	$W_U\%$	ORTHO	P95	>?
P-70M	25%	96%	0.175	0.177	✗
	50%	96%	0.118	0.122	✗
	75%	96%	0.163	0.203	✗
	100%	96%	0.111	0.198	✗
P-410M	25%	27%	0.146	0.157	✗
	50%	27%	0.238	0.251	✗
	75%	27%	0.190	0.216	✗
	100%	27%	0.201	0.209	✗
P-1B	25%	21%	0.159	0.167	✗
	50%	21%	0.193	0.205	✗
	75%	21%	0.242	0.269	✗
	100%	21%	0.186	0.193	✗

B Extended Quantitative Results

B.1 Model-Specific Geometric Profiles

Pythia-2.8B $d=2560, L=32$. Predictive organization is maintained across all layers ($z > 2$ at 32/33 layers). Peak $z = +14.5$ at L15; minimum $z = +0.4$ at L0 (embedding layer). No collapse observed. Late layers show gradual decline from peak but remain positive throughout, with recovery at the final layer ($z = +8.6$).

OLMo-1B $d=2048, L=16$ (trained on Dolma with tied embeddings). Strong predictive organization throughout: $z > 2$ at all 17 layers, $z > 5$ at 13/17 layers. Peak $z = +24.0$ at L15. The monotonically increasing profile in late layers contrasts with Pythia-1B’s plateau, possibly reflecting architectural differences (tied vs. untied embeddings). No loss of organization observed, consistent with the capacity interpretation given $d=2048$.

Pythia-6.9B $d=4096, L=32$. Peak $z = +17.93$ at L9. No mid- or late-layer masking, consistent with the other large Pythia models.

Phi-1.5 $d=2048, L=24$ (trained on textbook-quality data). Peak $z = +12.39$ at L24. No intermediate-layer collapse, consistent with the $d \geq 2048$ threshold.

Gemma-2-2B $d=2304, L=26$ (tied embeddings). Strong organization at intermediate layers (peak $z = +16.36$ at L22) but collapses at the final layer ($z = -16.5$ at L26). Because embeddings are tied, W_U must serve dual roles (input embedding and output projection), which may create tension at the output layer not present in untied models.

B.2 Comprehensive Numeric Tables

This section provides exact numeric values corresponding to the visualizations in the main text. Table 2 provides peak and trough z -scores across the complete model suite (corresponding to Figure 2a). Table 3 and Table 4 provide z -scores throughout training for Pythia-410M, 160M, and 1B (corresponding to Figure 4).

Table 2: **Predictive Organization Across Scales.** Mid-layer geometry is significantly organized for prediction in all models with sufficient depth. Small models lose this organization at late layers; large models maintain it throughout. P = Pythia, G = Gemma-2, O = OLMo. All results: $k=100$, 100 random subspaces, 1000 contexts.

MODEL	d	L	PEAK z	@ L	$z>5$	$z>2$	LATE-LAYER LOSS?
P-70M	512	6	+16.26	L6	1/7	2/7	YES ($z \rightarrow -11$, L3-5)
P-160M	768	12	+15.07	L12	1/13	4/13	YES ($z \rightarrow -13$, L8-11)
P-410M	1024	24	+9.27	L24	9/25	16/25	YES ($z \rightarrow -32$, L20-23)
P-1B	2048	16	+12.85	L8	14/17	16/17	NO
P-1.4B	2048	24	+12.34	L12	12/25	17/25	BORDERLINE ($z = -0.5$, L20)
P-2.8B	2560	32	+14.53	L15	23/33	32/33	NO
P-6.9B	4096	32	+17.93	L9	28/33	32/33	NO
PHI-1.5	2048	24	+12.39	L24	15/25	24/25	NO (LATE)
O-1B	2048	16	+24.00	L15	13/17	17/17	NO
G-2-2B	2304	26	+16.36	L22	26/27	26/27	FINAL ONLY ($z = -16.5$, L26)

Table 3: **Training Dynamics (Pythia-410M).** Predictive organization is established by step 512 (24/25 layers with $z>2$). Loss of organization appears after step 64,000 and deepens through the end of training, even as loss continues to improve.

STEP	$z>2$	PEAK z	MIN z	MASKED?
0	1/25	+2.1	-1.0	NO
512	24/25	+10.8	+0.1	NO
1,000	24/25	+20.4	+0.6	NO
4,000	22/25	+20.5	+0.3	NO
16,000	23/25	+18.4	-0.7	NO
64,000	19/25	+10.1	-0.5	NO
96,000	16/25	+8.1	-10.2	YES
143,000	16/25	+9.3	-32.3	YES

Table 4: **Multi-Model Training Dynamics.** 160M develops masking at the same time as 410M (step $\sim 96k$). 1B never develops masking despite comparable PC1 migration, supporting the capacity interpretation.

STEP	160M ($d=768$)		410M ($d=1024$)		1B ($d=2048$)	
	$z>2$	MIN z	$z>2$	MIN z	$z>2$	MIN z
0	0/13	-1.1	1/25	-1.0	0/17	-2.0
512	12/13	-0.2	24/25	+0.1	16/17	+0.2
1,000	12/13	+0.5	24/25	+0.6	16/17	+0.8
4,000	12/13	+0.5	22/25	+0.3	15/17	-1.0
16,000	8/13	-1.4	23/25	-0.7	15/17	+0.1
64,000	8/13	-1.4	19/25	-0.5	16/17	+0.1
96,000	7/13	-14.8	16/25	-10.2	16/17	-0.5
143,000	4/13	-13.0	16/25	-32.3	16/17	-0.8

C Robustness and Methodological Controls

C.1 Synthetic Validation

To test Subspace PGA independently of natural language, we generated synthetic sequences using 3, 5, and 8-state Hidden Markov Models alongside 1-, 2-, and 3-gram finite Markov chains. By feeding these tokens through our analytical pipeline, Subspace PGA consistently recovers the mathematically guaranteed state-transition boundaries ($r > 0.92$ on HMM clustering; Adjusted Rand Index = 1.0 for shallow Markov orders). This confirms that Subspace PGA can detect predictive structure independently of natural language complexity. See Table 5.

Table 5: Synthetic Validation.

PROCESS	CONFIG	SCORE	STD.
HMM (r)	3 STATES	0.980	± 0.00
	5 STATES	0.948	± 0.01
	8 STATES	0.929	± 0.02
MARKOV (ARI)	$n=1$	1.000	± 0.00
	$n=2$	1.000	± 0.00
	$n=3$	0.804	± 0.03

C.2 Anisotropy Correction

After mean+CCR-1, pairwise isotropy ≥ 0.99 for all models at all layers. Isotropy is computed as $1 - \lambda_1 / \sum_i \lambda_i$ where λ_i are eigenvalues of the pairwise cosine similarity matrix. Pre-correction, isotropy ranges from 0.78 (early layers) to 0.94 (mid layers); post-correction, all layers reach ≥ 0.99 , confirming the anisotropy is resolved.

C.3 CCR-1 / Readout Overlap

The CCR-1 correction removes the direction v_1 of largest variance in the centered hidden states. To check that this direction is largely outside the readout subspace—so that CCR-1 is not silently removing readout-aligned variance and biasing z —we report two complementary measures.

The primary measure (used in §3.2) is $\|P_k v_1\|$, the magnitude of v_1 ’s projection onto the readout subspace \mathcal{V}_k at $k=100$. At the layers where collapse occurs, this quantity is small: $\|P_k v_1\| \approx 0.13$ for Pythia-410M (L6–L23) and ≈ 0.25 for Pythia-1B. For reference, a uniformly random direction has expected projection norm $\sqrt{k/d}$, which is 0.31 for Pythia-410M and 0.22 for Pythia-1B—so 410M’s v_1 is more orthogonal to the readout than chance, and 1B’s is roughly at chance. At the final layer of both models, $\|P_k v_1\|$ rises to ≈ 0.42 – 0.55 (where $z > 0$). CCR-1 therefore removes a direction that lies mostly outside the readout at the layers where collapse happens, so any change in z after correction reflects geometric reorganization rather than removal of readout-aligned variance.

The second measure is the single-vector cosine $|\cos(v_1, u_1^{W_U})|$ —how much v_1 aligns with W_U ’s top right singular vector alone. This is a strict lower bound on $\|P_k v_1\|$ but easier to summarize per model. Table 6 reports $\max_\ell |\cos(v_1^{(\ell)}, u_1^{W_U})|$ across all layers for the Pythia suite. All values are < 0.18 , consistent with the projection-norm argument above.

Additional robustness checks (different random seeds, $k \in \{50, 200\}$, $k=d/10$) are reported inline in §4.1.

C.4 Unembedding Spectral Concentration

Figure 6 plots the cumulative variance explained by the top- k right singular vectors of W_U for all seven Pythia models. Small models (70M, 160M) have near-rank-1 unembedding

Table 6: **CCR-1 / readout single-vector overlap.** Maximum single-vector cosine $|\cos(v_1, u_1^{W_U})|$ across layers—a lower bound on $\|P_k v_1\|$ that summarizes CCR-1 / readout overlap per model.

MODEL	MAX $ \cos(v_1, u_1^{W_U}) $	LAYER
P-160M	0.060	L0
P-410M	0.134	L19
P-1B	0.122	L14
P-2.8B	0.173	L29

matrices: the top singular value alone explains $\sim 92\%$ of variance, and $k=100$ captures effectively all informative directions. Larger models have progressively flatter spectra ($k=100$ captures $\sim 30\%$ for 410M, $\sim 20\%$ for 1B). This steep spectral decay in small models is not an artifact—it reflects the limited capacity of W_U when d is small relative to $|\mathcal{V}|$. The $k=100$ readout subspace at 96% coverage in 70M *should favor* alignment, making the observed loss of predictive organization a conservative finding (§3.3).

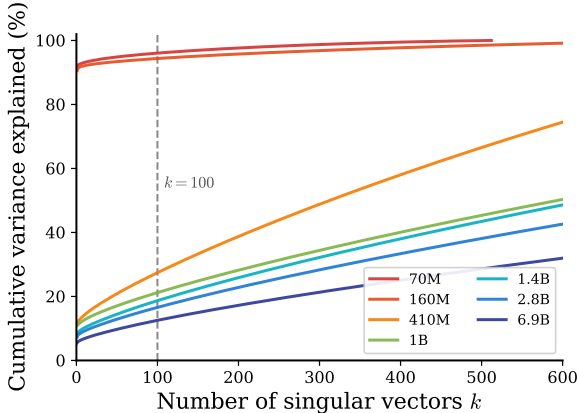


Figure 6: **Cumulative variance explained by top- k right singular vectors of W_U .** Small models (warm colors) have steeply decaying spectra; large models (cool colors) have flatter spectra. Dashed line marks $k=100$, the default readout subspace dimension.

C.5 Absolute Correlation Values Per Layer

Table 7 reports the absolute readout correlation ρ_{read} , null distribution mean μ_{null} and standard deviation σ_{null} , and z-score for every layer of four representative Pythia models. This contextualizes large-magnitude z-scores: at Pythia-410M L21 ($z = -32.3$), $\sigma_{\text{null}} = 0.0125$ is small but the absolute gap ($\rho_{\text{read}} = 0.499$ vs. $\mu_{\text{null}} = 0.903$) is large—the effect is substantive, not an artifact of vanishing σ_{null} .

C.6 Bootstrap Confidence Intervals

To assess the statistical reliability of our z-score estimates, we computed bootstrap confidence intervals by resampling the 1,000-text evaluation set with replacement (1,000 resamples) and recomputing Subspace PGA at representative layers for all five models. Table 8 reports point estimates and 95% bootstrap CIs for peak-alignment, trough (collapse), and final layers.

C.7 Sample Stability

To verify that results do not depend on the specific sample size used ($N=1000$), we evaluated Subspace PGA on Pythia-410M at $N \in \{100, 200, 500, 1000\}$, repeating each sample size 5

Table 7: **Per-layer absolute correlation values.** ρ_{read} : readout subspace Spearman correlation; $\mu_{\text{null}}, \sigma_{\text{null}}$: null distribution statistics from 100 random subspaces. Layers with $z < 0$ are **bolded**.

Model	Layer	ρ_{read}	μ_{null}	σ_{null}	z
P-160M	0	0.746	0.753	0.0197	-0.4
	5	0.743	0.655	0.0179	4.9
	8	0.736	0.887	0.0118	-12.8
	10	0.637	0.804	0.0155	-10.8
	12	0.850	0.599	0.0167	15.1
P-410M	7	0.581	0.509	0.0134	5.4
	14	0.755	0.649	0.0234	4.5
	18	0.768	0.652	0.0218	5.3
	20	0.650	0.857	0.0173	-12.0
	21	0.499	0.903	0.0125	-32.3
	23	0.615	0.834	0.0148	-14.8
	24	0.887	0.709	0.0192	9.3
P-1B	0	0.704	0.719	0.0191	-0.8
	5	0.600	0.448	0.0163	9.4
	8	0.635	0.445	0.0148	12.9
	12	0.831	0.573	0.0207	12.4
	16	0.872	0.711	0.0227	7.1
P-2.8B	0	0.711	0.703	0.0212	0.4
	6	0.519	0.392	0.0100	12.7
	15	0.625	0.406	0.0151	14.5
	24	0.810	0.712	0.0336	2.9
	32	0.860	0.661	0.0231	8.6

Table 8: **Bootstrap 95% CIs for Subspace PGA z-scores.** 1,000 bootstrap resamples per model. Peak = layer with highest z ; trough = layer with lowest z (collapse zone for small models); final = last layer. CIs confirm that collapse in small models and alignment in large models are not sampling artifacts.

MODEL	LAYER	z -SCORE	95% CI
P-160M	PEAK/FINAL (L12)	+15.1	[+13.7, +16.1]
	TROUGH (L8)	-12.8	[-13.6, -11.7]
P-410M	PEAK/FINAL (L24)	+9.3	[+8.6, +9.8]
	TROUGH (L21)	-32.3	[-35.0, -29.1]
P-1B	PEAK (L8)	+12.9	[+11.6, +13.4]
	FINAL (L16)	+7.1	[+6.5, +7.6]
P-2.8B	PEAK (L15)	+14.5	[+13.1, +15.2]
	FINAL (L32)	+8.6	[+7.9, +9.1]
O-1B	PEAK (L15)	+24.0	[+21.1, +25.2]
	FINAL (L16)	+14.4	[+13.0, +15.2]

times with different random text subsets. Table 9 reports mean and standard deviation of z -scores across repeats at the peak (= final, L24) and trough (L21) layers. Since peak and final coincide for Pythia-410M, they share one row.

C.8 Specificity to the Predictive Interface (W_E Control)

A natural concern is whether *any* embedding matrix would produce comparable alignment, rather than specifically W_U . We test this by computing Subspace PGA using the input embedding matrix W_E (which participates in tokenization, not prediction) in place of W_U for Pythia-410M, 1B, and 160M—all models with untied embeddings where $W_E \neq W_U$. The

Table 9: **Sample Stability (Pythia-410M)**. z-scores (mean \pm std, 5 repeats) are stable across sample sizes. Collapse is detectable even at $N=100$.

LAYER	$N=100$	$N=200$	$N=500$	$N=1000$
PEAK/FINAL(L24)	$+8.5\pm 0.8$	$+9.1\pm 0.7$	$+9.6\pm 0.8$	$+9.8\pm 0.9$
TROUGH(L21)	-30.2 ± 4.7	-35.2 ± 4.8	-35.0 ± 3.7	-33.3 ± 1.6

top-100 SVD subspaces of W_U and W_E are nearly orthogonal (Grassmann overlap 0.10 for Pythia-410M, 0.05 for Pythia-1B), confirming these are genuinely different subspaces. The contrast is clear: W_U produces mean $|z| = 6.5$ (410M) and 8.6 (1B), while W_E produces mean $|z| = 1.0$ for both—statistically indistinguishable from random subspaces. At individual layers, W_U z-scores reach $+9.3$ (410M final layer) and -32.3 (410M L21), while all W_E z-scores remain in the range $[-0.7, +1.8]$ (excluding L0, where $z_{W_E} = +6.2$ is expected since layer-0 representations *are* the input embeddings). Geometry is organized specifically for prediction through the learned output interface, not for any matrix the model happens to contain.

D Theoretical Dissociations and Mechanisms

D.1 Content-Dependent Organization (JSD-Based PGA)

Using JSD-based PGA, deep-processed content shows positive PGA while shallow-processed content shows near-zero or negative PGA in 7/8 models after entropy control. **Note:** JSD-based PGA is valid for comparing content types (same readout) but not for learned-vs-random readout comparison due to distributional confounds.

Table 10: **Content-Dependent PGA (JSD-Based)**. 7/8 models significant after entropy control.

MODEL	Δ_{raw}	p	Δ_{pCorr}	p
P-70M	+1.97	<.001	+1.136	<.001
P-160M	+1.184	<.001	+1.137	<.001
P-410M	+4.52	<.001	+3.318	<.001
P-1B	+2.82	<.001	+2.209	<.001
P-2.8B	+3.21	<.001	+2.237	<.001
P-6.9B	+2.44	<.001	+2.206	<.001
O-1B	+1.186	<.001	+1.113	<.001
O-7B	+0.037	.038	-.011	.749

D.2 Causal Intervention

Displacing hidden states toward a target context shifts next-token predictions directionally, specifically, and proportionally to displacement magnitude. Random-direction and PC1 controls show minimal effect, confirming specificity to semantic content. We extract hidden states at peak-z layers, inject a displacement vector toward an independent target context, and measure prediction shift. This shifts probability mass toward the target without modifying weights, confirming that the geometric orientation measured by Subspace PGA is functionally relevant.

D.3 Logit Lens Failure vs. Loss of Predictive Organization

The logit lens evaluates absolute decodability (whether W_U maps a hidden state to the correct token); Subspace PGA evaluates distance-structure alignment. Figure 7 shows these dissociate: all models exhibit logit lens failure at intermediate depths, but large models

maintain positive Subspace PGA through this zone—geometric structure remains organized for prediction even when absolute coordinates have drifted.

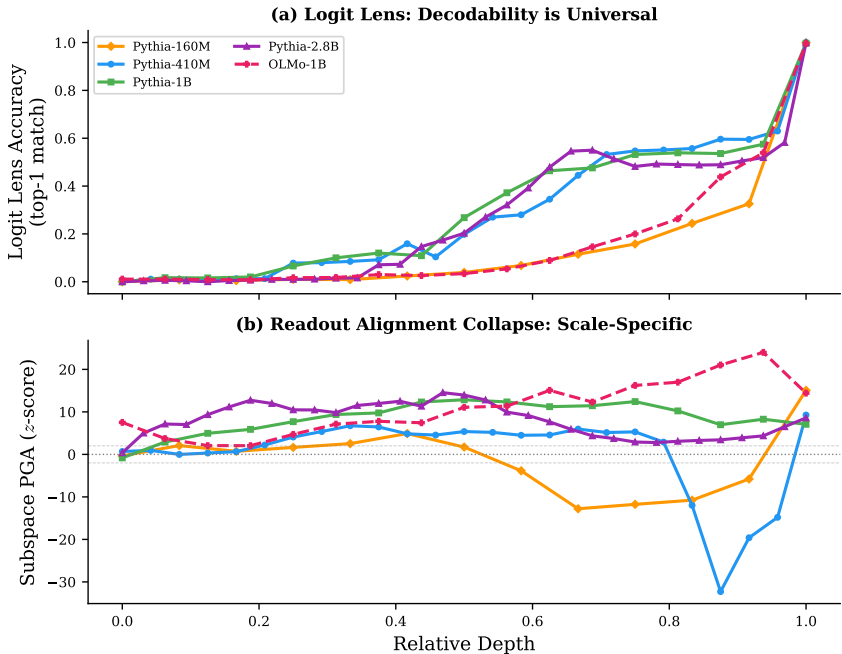


Figure 7: **Logit Lens vs Subspace PGA.** (a) Absolute decodability fails universally at intermediate depths. (b) Intrinsic geometric organization collapses only in small-capacity models. The dissociation confirms that geometric organization for prediction and absolute decodability are distinct properties.

D.4 Spectral Metrics Are Blind to Predictive Organization

Spectral metrics (e.g., α -ReQ, RankMe) characterize the shape of a representation manifold, but Figure 8 shows they do not reliably predict functional organization.

The dissociation occurs because spectral metrics measure the *intrinsic shape* of the coordinate space (the variance decay profile across principal components), while Subspace PGA measures the *extrinsic orientation* of that space relative to the functional readout (W_U). When a small-capacity model undergoes the geometric detour, its internal manifold rotates away from the predictive interface. Because this operates as a near-rigid coordinate transformation, the internal eigenvalue density remains largely unchanged (α -ReQ stays flat) even as functional alignment collapses.

D.5 KL Projection Analysis

To test whether prediction-irrelevant directions carry functional information, we projected hidden states into the readout subspace at each layer and measured the effect on next-token predictions. Late layers of small models are *least* sensitive to this projection (KL = 3.6, 32.5% top-1 agreement preserved at Pythia-410M L21), while mid-layers are highly sensitive (KL = 8.8 at L8). The prediction-irrelevant computation at affected layers does not carry crucial predictive information; it is geometric reorganization, not novel prediction. By contrast, Pythia-1B at equivalent relative depth shows KL = 4.2 but only 12.5% top-1 agreement, suggesting that large models’ non-predictive computation at equivalent depth carries more functional weight.

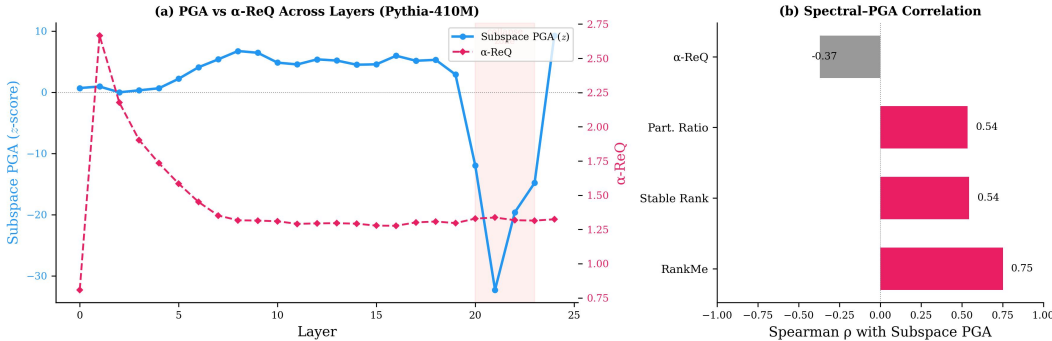


Figure 8: **Spectral Metrics Are Blind to Predictive Organization.** (a) Subspace PGA z-score and α -ReQ across layers (Pythia-410M). α -ReQ is flat through the zone where predictive organization collapses (shaded) despite a >40 -standard-deviation PGA swing. (b) Spearman correlation between each spectral metric and Subspace PGA z-scores across layers. Correlations are model-dependent; no metric is a consistent predictor across the suite.

D.6 Theoretical Connections

Computational mechanics (Crutchfield & Young, 1989) predicts that optimal prediction requires grouping histories with identical conditional futures. Positive Subspace PGA is consistent with this at mid-layers; the loss of predictive organization at late layers of small models establishes an empirical boundary the theory does not specify. Zhao et al. (2024)’s implicit alignment theorem predicts collinear representations for contexts sharing next-token support—our results show this holds at most layers but breaks down where anisotropy overwhelms the predictive signal. The loss of predictive organization in small models’ late-but-not-final layers also poses a question under Saurez et al.’s invariant subspace theorem: the architectural necessity of W_U -aligned features appears to be fully satisfied only at the final layer.

The information bottleneck (Tishby et al., 1999) provides a framework for finding maximally compressed representations that preserve task-relevant information; Shwartz-Ziv & Tishby (2017) applied this to neural networks and reported a compression phase in training. Our training dynamics show *selective* compression: continued training compresses small models’ late-layer geometry into prediction-irrelevant directions, reducing functional organization even as loss improves. This is compression, but not toward prediction—a nuance the bottleneck framework does not distinguish.

The linear representation hypothesis (Park et al., 2024) assumes that geometric proximity reflects functional similarity. Our results qualify this: it holds at most layers of all models, but at late layers of small models, the dominant geometric directions are orthogonal to prediction. Geometric proximity there reflects non-predictive similarity.

E Experimental Details

Context Sampling We sample 1,000 texts from OpenWebText, filtering for ≥ 64 tokens and truncating to 512 tokens. To avoid autocorrelation between tokens within a sequence, we use only the *final-token* hidden state from each of the 1,000 independent contexts.

CCR-1 Estimation Requirements CCR-1 requires estimating the top eigenvector of the covariance matrix. With $N=1,000$ independent samples, this estimate is stable even at $d=4096$ (Pythia-6.9B), since only the leading eigenvector (not the full covariance) is needed.

Statistical Methodology Pairwise distance matrices violate independence assumptions required by parametric tests. We therefore use *Mantel permutation tests* (Mantel, 1967) with

$B=1,000$ random permutations to derive non-parametric null distributions for all distance-matrix correlations.

Compute and Hardware All experiments use PyTorch and HuggingFace Transformers. Total compute: approximately 60–80 A100 GPU-hours across the full Pythia suite, cross-architecture models, and multi-checkpoint training dynamics.